ACS APPLIED MATERIALS & INTERFACES

www.acsami.org

Research Article

All-Day, All-Weather Desalination Using a Contactless Evaporator with Antisalt Fouling Property

Higgins M. Wilson, Tawseef A. Wani, and Sang J. Lee*

Cite This: https://doi.org/10.1021/acsami.4c17002

Read Online

ACCESS | Metrics & More | Article Recommendations | Supporting Information

ABSTRACT: Interfacial solar steam generation (ISSG) technology provides a promising solution to the global issue of freshwater scarcity. However, its practical application is hindered by salt fouling and inconsistent solar illumination. In this work, a novel interfacial solar steam generator is proposed that integrates contactless design with low-voltage joule heating to provide all-day, all-weather freshwater generation. The contactless design utilizes a solar-reduced graphene oxide coated carbon fabric (SRGO−CF) as a heat generator and super hydrophilic paper walls as water transport channels. The contactless device can generate steam at the maximum rate of 4.27 kg m^{-2} h^{-1} under 1 sun solar illumination and small input voltage due to the excellent photothermal and electrothermal capabilities of SRGO−CF. At an input voltage of 2.5 V, the SRGO−CF evaporator exhibits an evaporation rate of 3.52 kg m^{-2} h^{-1} and 2.32 kg m^{-2} h^{-1} for 3.5 wt % salt water respectively with and without 1 sun illumination for a long period of time without any salt fouling, demonstrating its all-day, all-weather capability. The proposed contactless ISSG evaporator can resolve the impractical issue of conventional ISSG-based evaporators owing to irregular weather conditions and salt fouling issues while also promoting zero liquid discharge-based salt harvesting.

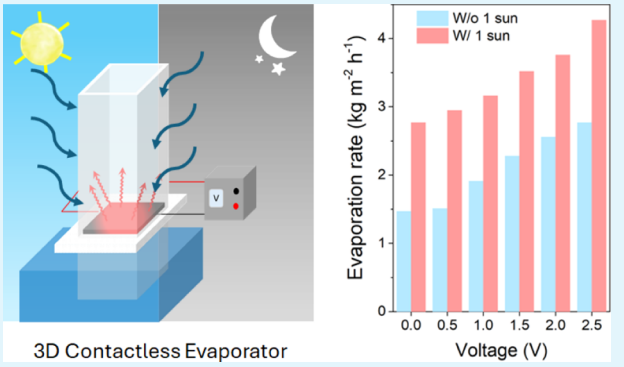

KEYWORDS: *contactless, joule heating, solar desalination, interfacial heating, solar reduced graphene oxide*

INTRODUCTION

The global issue of global water scarcity is escalating, owing to climate change and population growth. The development of innovative water purification technologies is necessitated.[1,2] Although conventional methods, such as reverse osmosis are effective, they are hindered by high energy demands and significant financial costs.[3] A promising alternative lies in interfacial solar desalination technology, which offers the potential to significantly reduce both energy consumption and costs, making it particularly advantageous for regions with limited resources.[4] Notably, interfacial solar steam generation (ISSG) has garnered large attention due to its unique capability to operate efficiently under solar illumination, a distinct advantage over traditional bulk water heating methods.[5] However, the practical deployment of ISSG faces several challenges, including salt accumulation, vulnerability to weather fluctuations, and suboptimal water collection efficiencies.[6,7] Addressing these challenges is essential for the successful and widespread implementation of ISSG technology in practical applications.[8]

To address the challenge of salt accumulation in ISSG desalination systems, several strategies have been introduced, focusing on salt resistance, controlled salt precipitation, and self-cleaning. Salt resistance can be achieved by optimizing surface wettability and porous structures, as seen in self-descaling Janus evaporators, which use thermoresponsive materials to repel seawater and facilitate efficient rinsing.[9] Self-cleaning mechanisms include rotatable evaporators in cylindrical or spherical shapes that periodically rotate to dissolve and remove the accumulated salts, thereby maintaining consistent efficiency.[10] Controlled salt precipitation method introduces crystallization at specific regions. For example, a conical MXene-functionalized hydrogels minimizes salt buildup on critical surfaces.[11] Among these antisalt fouling strategies, the contactless salt mitigation approach has shown particular promise by separating the photothermal conversion surface from the evaporation surface to prevent salt contamination.[12−14] This contactless design transfers heat without direct contact or via radiative heating, promoting zero liquid discharge (ZLD) and keeping the photothermal surface free from fouling. Salt crystallization occurs on the water evaporation surface instead, ensuring that the photothermal layer remains free from fouling and maintains a stable

Received: October 3, 2024
Revised: November 20, 2024
Accepted: November 26, 2024

performance over time, even in highly saline environments. For instance, Chen et al. utilized a separated system which showcased long-term stable evaporation (1.25 kg m^{-2} h^{-1} under 1 kW m^{-2} (1 sun) illumination, 15 wt % $NaCl_{(aq)}$, ≥ 120 h) using a polypyrrole@Co_3O_4@aluminum sheet and a T-shaped superhydrophilic polyethylene/polypropylene nonwoven fabric right under the sheet.[13] However, the evaporation performance of these contactless evaporators has been relatively poor compared to those of other ISSG evaporators. Thus, further development of contactless evaporators is required to enhance the evaporation performance.

Recently, the Joule heating-assisted (JHA) ISSG technique has received significant attention due to its superior evaporation performance and ability to operate in all-day, all-weather conditions. The technique exhibited impressive evaporation performance regardless of weather conditions.[15−17] By operating at low input voltages, JHA evaporation devices achieved evaporation rates exceeding 10 kg m^{-2} h^{-1}, substantially surpassing rates limited by solar illumination alone. The integration of the low-voltage Joule heating method enhances overall evaporation performance owing to the synergistic effects of photothermal and electrothermal heating.[18] Electrothermal heating, in particular, is beneficial under adverse conditions such as nighttime or cloudy weather. This concept of continuous operation has been a historical challenge in ISSG-based solar stills to ensure a consistent supply of clean water.[19] However, the adoption of an effective all-day, all-weather JHA-ISSG device faces significant challenges, such as rapid salt accumulation at the air−water interface. As the evaporation rate increases with the aid of Joule heating, the amount of salt accumulation also rises, leading to issues such as salt fouling, corrosion, and degradation of the device, diminished evaporation performance, and poor long-term durability. Therefore, systematic efforts are needed to tackle these issues for practical all-day, all-weather desalination.

For efficient photothermal evaporation, materials with a broadband solar absorbance are a necessity. For this purpose, carbonaceous materials have been utilized extensively owing to their broadband light absorption, low cost, reusability, and excellent light-to-heat conversion properties.[20] Reduced graphene oxide (rGO) has been reported in numerous previous reports as an excellent photothermal absorber for ISSG.[21] In addition, rGO has outstanding electrical properties with large applications in energy storage, batteries, and so on.[22] Among these, solar-reduced graphene oxide (SRGO) has not yet been explored for solar thermal applications. Moreover, SRGO's high electrical conductivity suggests it could support efficient electrothermal heating, which is beneficial for high evaporation rates. Its scalable and rapid synthesis process, requiring no additional purification, makes it suitable for large-scale applications.[23] Despite its simple production, SRGO retains electrical properties comparable to those of other rGO, making it a promising candidate for scalable JHA-based ISG systems. In this study, a novel 3D contactless evaporator utilizing SRGO coated on carbon fabric (CF) is proposed for all-day, all-weather desalination with antisalt fouling. The SRGO−CF can effectively harness solar illumination and emit radiative heat to the surrounding walls for radiative heating-based evaporation. Due to the net energy gain of the tall paper walls of the proposed 3D evaporator, the SRGO−CF-*x* (*x*: height in cm) evaporator can evaporate water, breaking the theoretical limit of evaporation under 1 sun solar illumination. The supply of low-voltage increases the evaporation performance to 4.27 kg m^{-2} h^{-1} under 1 sun illumination and 2.5 V, owing to the excellent synergetic heat generation of SRGO−CF-5. When the SRGO−CF-5 evaporator is applied for seawater desalination, it generates steam at a high rate of 3.52 kg m^{-2} h^{-1}. The SRGO−CF-5 evaporator can be used for all-day, all-weather solar desalination, even under no solar illumination conditions. The present results address the issue of poor evaporation performance of conventional contactless evaporators, the impracticability of ISSG-based evaporators owing to weather conditions, and the salt fouling issue of traditional ISSG evaporators while also promoting zero liquid discharge-based salt harvesting.

EXPERIMENTAL SECTION

Materials. Graphene oxide (GO) solution with a concentration of 3 g/L, poly(vinylidene fluoride) (PVDF), and dimethylformamide (DMF) was purchased from Sigma-Aldrich, South Korea. CF, commercial copper tape, copper wire, and silver paste were provided by ABC, Korea. Paper filters utilized for water transport were purchased from Redclay humidifier, South Korea.

Fabrication of SRGO−CF. GO sheets were prepared by drying the purchased GO solution at room temperature for 2−3 days. Once dried, the GO sheets were reduced to SRGO by employing focused solar light using a convex lens. The successful reduction of the GO sheets to SRGO was confirmed by the color change from golden brown to black. After complete reduction was ensured, the resultant SRGO powder was collected and stored for future use.

Next, SRGO was coated onto CF by using a simple dip-coating method. To achieve this, 200 mg of SRGO was mixed with a 20 wt % solution of PVDF in 10 mL of DMF. This mixture was sonicated for 1 h to form a uniform SRGO ink. A 2 cm × 3 cm CF was cleaned with ethanol and water and then repeatedly dipped into the prepared SRGO ink, followed by drying to ensure proper coating of the material. The coated SRGO−CF was then dried overnight to ensure a firm attachment of SRGO to the CF.

Fabrication of the SRGO−CF-*x* Evaporator. The prepared SRGO−CF was connected to copper tape and copper wire to supply electric power. After the copper wires were secured, the SRGO−CF was mounted on a polystyrene foam base for insulation and structural support, and pins were used for attachment. Two slits were then made in the foam to accommodate filter paper strips, allowing them to extend into the underlying bulk water solution.

The filter paper was cut, as illustrated in Figure S2. The dimensions matched those of the evaporator to ensure the optimal enclosure of the SRGO−CF device. This maximizes the heat absorption while preventing direct contact with the water. The paper walls with different heights (ranging from 1 to 5 cm) were prepared to investigate the effect of 3D heating on the evaporator's performance.

Characterizations. The surface characteristics of GO and SRGO were assessed by employing high-resolution field emission scanning electron microscopy (FESEM, JSM 7800F Prime, JEOL, Ltd., Japan). The elemental compositions of GO and SRGO were investigated by using X-ray photoelectron spectroscopy (XPS, PHI 5000 VersaProbe III). Additionally, the crystal structures of these materials were examined by employing an X-ray diffractometer (D8 Advance DSVINCI, Bruker USA). Furthermore, the optical characteristics of the SRGO−CF evaporator were characterized using a UV−vis−NIR spectrometer (V-670, JASCO INC., Japan).

Steam Generation Experiment. The evaporation performance of the SRGO−CF-*x* devices was evaluated using a AAA solar simulator (PEC, L-101, Korea) under controlled conditions in an air-conditioned room maintaining a constant temperature of 27 °C and 50% humidity. An SRGO−CF-*x* evaporator with dimensions of 2 × 2 cm^2 was placed on a polystyrene foam, which provided thermal insulation, and it was positioned above bulk water contained in a beaker. The mass reduction of water was measured using an electronic analytical balance, while the device was exposed to a solar intensity of

https://doi.org/10.1021/acsami.4c17002
ACS Appl. Mater. Interfaces XXXX, XXX, XXX−XXX

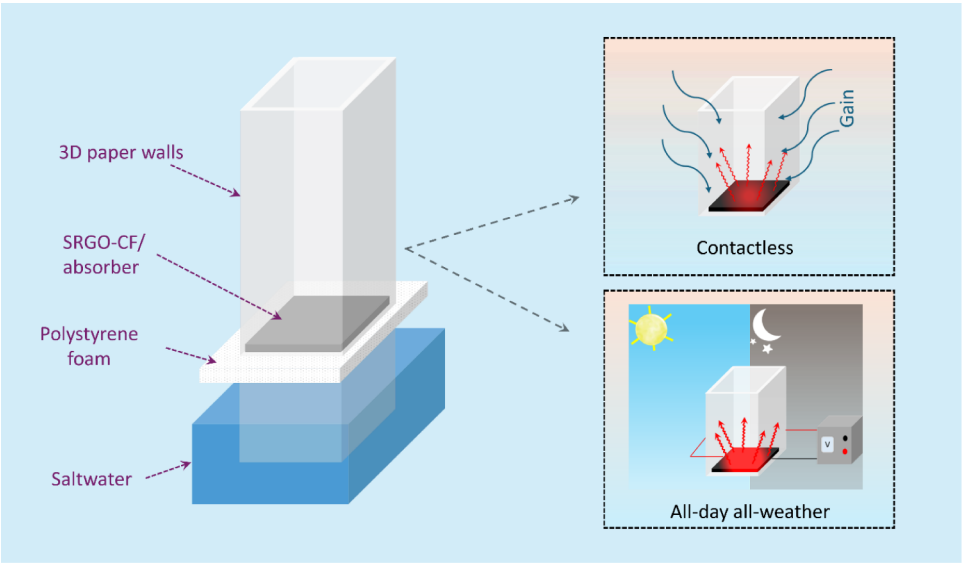

Figure 1. Schematic diagram of the SRGO−CF-*x* contactless steam generator.

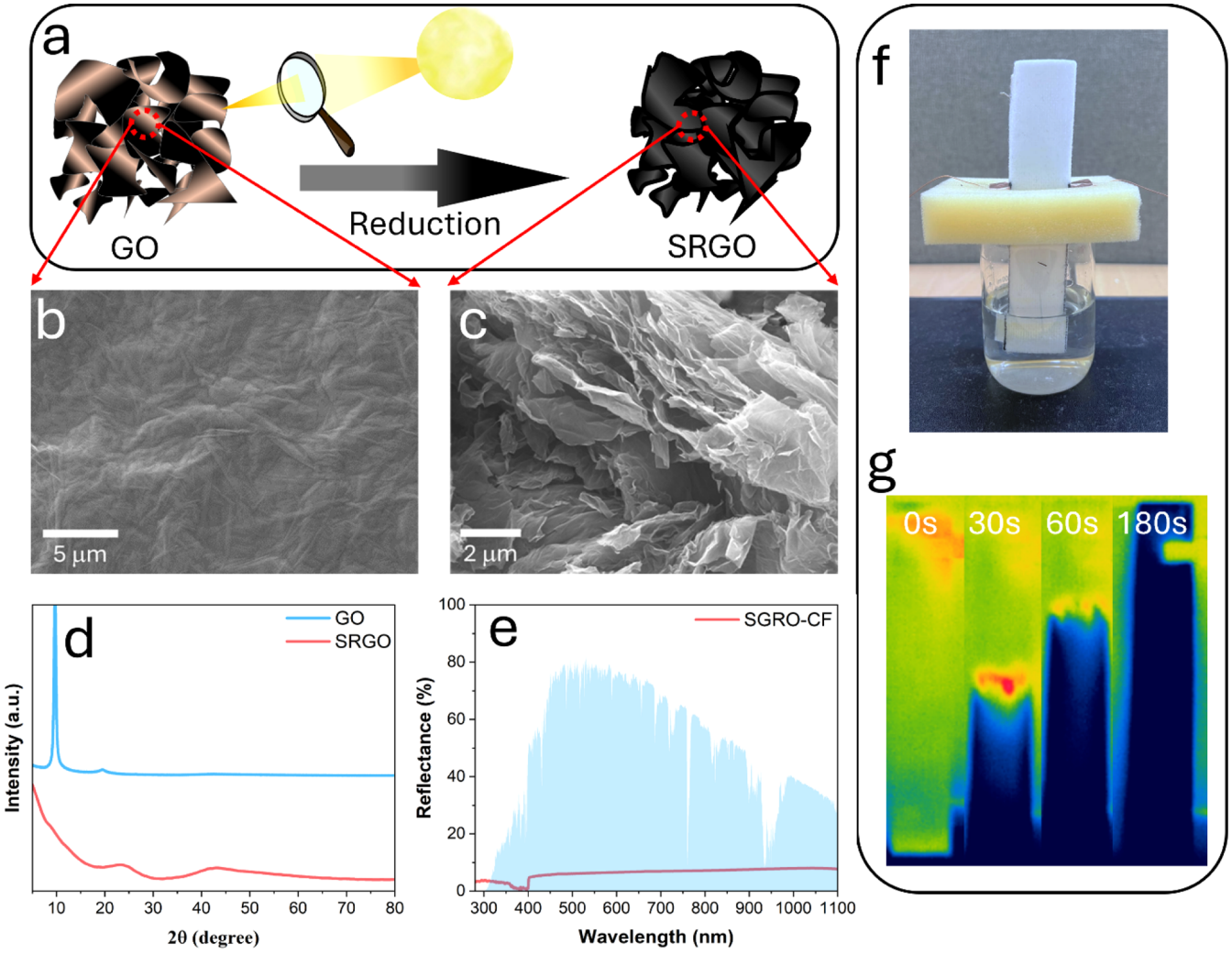

Figure 2. (a) Schematic diagram showing the reduction of GO to SRGO. SEM images of (b) GO and (c) SRGO. (d) XRD spectra of GO and SRGO. (e) Absorption spectra of the SRGO−CF. (f) Digital photograph of the SRGO−CF-*x* steam generator. (g) IR thermal images showing the rapid water transport through the surrounding paper walls.

https://doi.org/10.1021/acsami.4c17002
ACS Appl. Mater. Interfaces XXXX, XXX, XXX−XXX

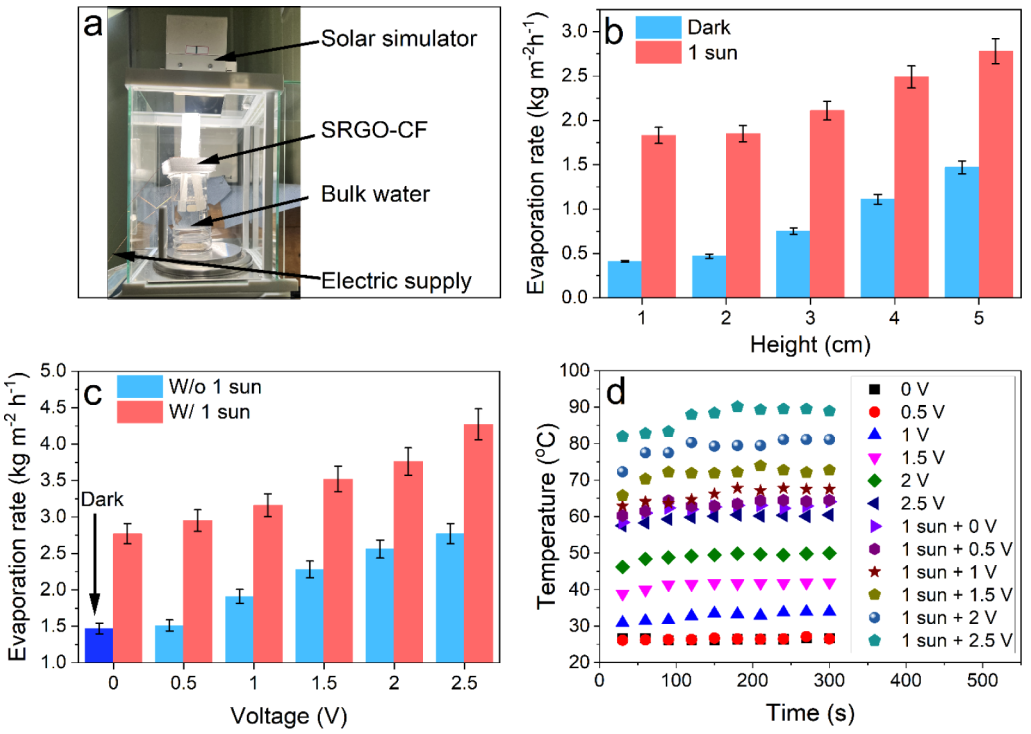

Figure 3. (a) Digital photograph of the experimental setup of solar steam generation. (b) Evaporation rates of SRGO−CF-x (x = 1 to 5 cm) with and without 1 sun illumination. (c) Evaporation rates of SRGO−CF-5 devices under 1 sun illumination at various input voltages. (d) Temporal variations of the surface temperature of SRGO−CF-5 according to input voltage with and without 1 sun solar irradiation.

1 kW/m^2. An infrared (IR) thermal camera (FLIR-C3 IR camera, USA) was used to monitor the temperature variations on the device. The electrical power required for the experiment was supplied by a standard direct current (DC) power source (Smart, model RDP-305).

Solar Desalination Experiment. Similar to the water evaporation tests, the solar desalination performance of the proposed SRGO−CF-5 evaporator was evaluated by using a AAA solar simulator. Salt solutions with concentrations of 3.5 and 20 wt % were prepared for the desalination tests. These experiments were conducted under 1 sun illumination with and without the supplied input voltage. The mass reduction in water was continuously recorded by using an electronic analytical balance. Salt accumulation on the surface of the evaporator was monitored and visualized using SEM imaging to assess its antifouling properties.

RESULTS AND DISCUSSION

In conventional ISSG evaporators, the solar absorber is usually in direct contact with water at the air−water interface. Solar energy is converted to heat, which is then transferred to the contact water through thermal conduction, driving evaporation. However, this direct contact between the absorber and water often leads to salt deposition (fouling) on the absorber surface. Over time, this salt fouling reduces the evaporation performance, limiting the effectiveness of the evaporator in long-term use. On the other hand, contactless evaporators utilize radiative heating, where the absorber transfers heat to water indirectly.[24] Water has strong absorption in the IR region defined using the Beer−Lambert law which describes how a radiation beam is absorbed as it passes through an absorbing medium:

$$t_\lambda(l) = \frac{I_\lambda(l)}{I_\lambda(0)} = e^{-\beta_\lambda l} \quad (1)$$

where $t_\lambda(l)$ is the spectral transmittance, I_λ is the intensity of a beam at distance l, and β_λ is the spectral absorption coefficient. The reciprocal of β_λ, known as the penetration depth, signifies the ability of water to absorb the photons of wavelength λ. The infrared wavelengths penetrate to a depth of approximately 100 μm, where they are strongly absorbed due to their resonance with the vibrational energy of water molecules.

The radiative heating has shown lower evaporation efficiency compared to conduction-based heating, presenting challenges for real-world desalination applications.[12] Figure 1 illustrates the concept of a contactless evaporator designed to overcome this limitation by incorporating a JHA evaporation mechanism. The contactless solar steam generator, named SRGO−CF-x, is proposed to eliminate any direct contact with the heat generator (SRGO−CF) and the surrounding vertical walls of water transporting super hydrophilic filter paper.

Previous studies have extensively highlighted the exceptional solar broadband absorption and light-to-heat conversion properties of rGO, making it a highly effective material for photothermal solar desalination in ISSG systems.[25] Additionally, the excellent electrical conductivity of rGO has been demonstrated in various energy storage applications. Furthermore, rGO exhibits remarkable emissivity in the infrared wavelength range, making it particularly well-suited for radiative heating in steam generation.[26] One of the simplest and most chemical-free methods to rapidly reduce GO into rGO is to use concentrated sunlight with the help of a convex lens.[27] This technique not only facilitates rapid reduction but also preserves the excellent electrical properties of rGO. In this work, GO sheets were similarly reduced by using focused sunlight with the aid of a laboratory convex lens, as shown in Figure 2a. When the focused solar light passing through a convex lens falls on the GO surface, the increase in the surface temperature leads to the decomposition of the GO into

https://doi.org/10.1021/acsami.4c17002
ACS Appl. Mater. Interfaces XXXX, XXX, XXX−XXX

graphene and CO_2, with a minor formation of H_2O. This transformation from GO to rGO (named SRGO) was evident from the rapid color change from brown to black and rapid volume expansion of the material.

This rapid transformation was visualized by SEM imaging. The SEM images (Figure 2b,c) reveal the exfoliation of sheets, indicating successful separation into thinner layers. However, some degree of agglomeration and stacking is evident, likely due to van der Waals interactions between the sheets.[23] This formation was also further confirmed by powder XRD analysis. Figure 2d shows the obtained XRD pattern of GO before and after the focused solar light treatment. The sharp peak at 9.86° corresponds to the (002) reflection plain in GO.[28] However, after solar reduction, the peak disappears, and two new peaks are formed at 23.7° (002) and 42.7° (100), indicating the successful reduction of GO. XPS analysis was also utilized to further evaluate the reduction of the GO sheets (Figure S1). The survey scan shows a decrease in oxygen concentration in SRGO compared to GO. In addition, in the C 1*s* spectra, the C═C peak becomes more intense, while the peaks associated with C═O and C−O diminish, signifying the elimination of oxygen-containing functional groups and the formation of the graphitic C═C structure.[27] The light absorption capability of SRGO−CF was experimentally assessed using UV−vis−NIR diffuse reflectance spectra over a wavelength range of 250 to 1100 nm. As shown in Figure 2e, SRGO−CF shows a diffuse reflectance of less than 5% over a whole range of wavelengths. The prepared SRGO sample was then coated on a small piece of CF to fabricate SRGO−CF as described in the experimental section. The contactless evaporator (SRGO−CF-*x*) was completed by adding water transport channels around SRGO−CF while ensuring no direct contact (Figure S2). The water transport channels were made of super hydrophilic rapid water transporting filter paper. As illustrated in Figure 2f,g, the water channels of 12 cm in height can transport water to the top from the bulk solution within 180 s. This is due to the paper composition which consists of a large number of cellulose fibers of average size ∼10 μm (Figure S3). The SRGO added with water transporting channels was connected to the bulk solution by using a polystyrene foam as insulation and support.

Figure 3a illustrates the experimental setup utilized for evaluating the steam generation performance. As described in the experimental section, the SRGO−CF was designed specifically to isolate it from direct contact with bulk water and water transporting surrounding walls. It should be noted that the surrounding walls in contactless design should be able to capture the radiative heat emitted by the absorber. As reported in previous literature, a high radiative view factor (F) is crucial for enhancing the absorption of emitted thermal energy.[24] Theoretical calculations showed that a height greater than >4 cm can achieve a high radiative view factor of >98% for an evaporative surface of dimensions 2 cm × 2 cm. For comparison of performance, 5 different heights (1 to 5 cm) were selected for the surrounding walls. Figure 3b shows the dark evaporation rate at each height. The dark evaporation rate is 0.41 kg m^{-2} h^{-1} for a 1 cm wall height and increases to 0.47, 0.75, 1.15, and 1.47 kg m^{-2} h^{-1} for 2, 3, 4, and 5 cm walls, respectively. As the wall height increases, the dark evaporation rates are also increased. This is attributed to the much lower temperature of the walls compared to the surrounding temperature of the 3D device. As height increases, the effective surface area increases, leading to the net convective and radiative energy gain from the hotter surroundings. The captured thermal images (Figure S4) also show a temperature 4−5 °C lower than the surrounding room temperature (∼27.3 °C), confirming the net energy gain. Under 1 sun illumination, the evaporation rate shows a similar trend, with evaporation rates increasing from 1.83 kg m^{-2} h^{-1} (1 cm) to 1.85, 2.11, 2.49, and 2.78 kg m^{-2} h^{-1} for heights 2, 3, 4, and 5 cm, respectively. The evaporation rates are all much higher than the theoretical limit (1.47 kg m^{-2} h^{-1}) for 1 sun illumination, indicating the net energy gain of the 3D evaporators. This was also the case in lower solar intensities as well (Figure S5). This net energy gain can be explained via energy exchange analysis, as illustrated in Table S1. The total energy loss, including both convective and radiative losses, is estimated to be 0.094 W. As the height of the evaporator increases, the net energy gain progressively increases to 0.054, 0.1083, 0.1624, and 0.2165 W for evaporators with heights of 2, 3, 4, and 5 cm, respectively. This confirms the correlation between the energy gain and enhanced evaporation performance with increased evaporator height. Moreover, the thermal efficiency of the evaporator is improved with height, reaching 79.2%, 81.5%, 83.2%, and 84.75% for the heights 2, 3, 4, and 5 cm configurations, respectively. These results are well aligned with the corresponding solar-to-vapor efficiencies of each evaporator, further validating the enhanced performance with taller evaporators.

Although the evaporation rates under 1 sun illumination are high in 3D evaporators, their evaporation performance largely depends on the input solar illumination. The solar illumination in most practical situations is inconsistent due to weather conditions. Therefore, it is imperative to offset this inconsistent variation with the addition of consistent input energy such as low-voltage electric power. In previous reports, the addition of joule heating has significantly enhanced the evaporation performance due to synergetic photoelectrothermal heating.[29] Figure 3c demonstrates the increased evaporation rate of SRGO−CF-5 under 1 sun illumination for different input voltages (0.5−2.5 V). The supply of low input energy enhances the evaporation rates to 2.95, 3.16, 3.52, 3.76, and 4.27 kg m^{-2} h^{-1} for input voltages of 0.5, 1, 1.5, 2, and 2.5 V, respectively. The evaporation rate is almost ∼150% increased with an input voltage of 2.5 V. The input voltage of the SRGO−CF-5 evaporator was not increased above 2.5 V to limit the reliance on electrical power input and the possible instability of polystyrene foam at higher temperatures, hindering the long-term operations of the SRGO−CF-5 evaporator. The evaporation rate of SRGO−CF-5 due to joule heating electrothermal evaporation was also evaluated. The evaporation rate increases to 2.77 kg m^{-2} h^{-1} at 2.5 V input voltage, underscoring the ability of the SRGO−CF-5 evaporator as a standalone joule heating-induced steam generator, which is advantageous in the design of ISG evaporators operating under diverse environmental conditions. The joule heating-induced evaporation performance was visualized by IR thermal images, as shown in Figure S6. Despite the evaporator having a contactless configuration, the addition of a low input voltage impacts the evaporation performance significantly. With the increase of input voltages, the maximum temperatures of the walls are increased. For instance, the temperature increases from 31.3 °C for 1 sun only to 42.7 °C with the addition of a 2.5 V input voltage. In addition, a notable expansion of the hotter region is observed with an increasing input voltage. This is mainly attributed to the increase in the surface temperature

https://doi.org/10.1021/acsami.4c17002
ACS Appl. Mater. Interfaces XXXX, XXX, XXX−XXX

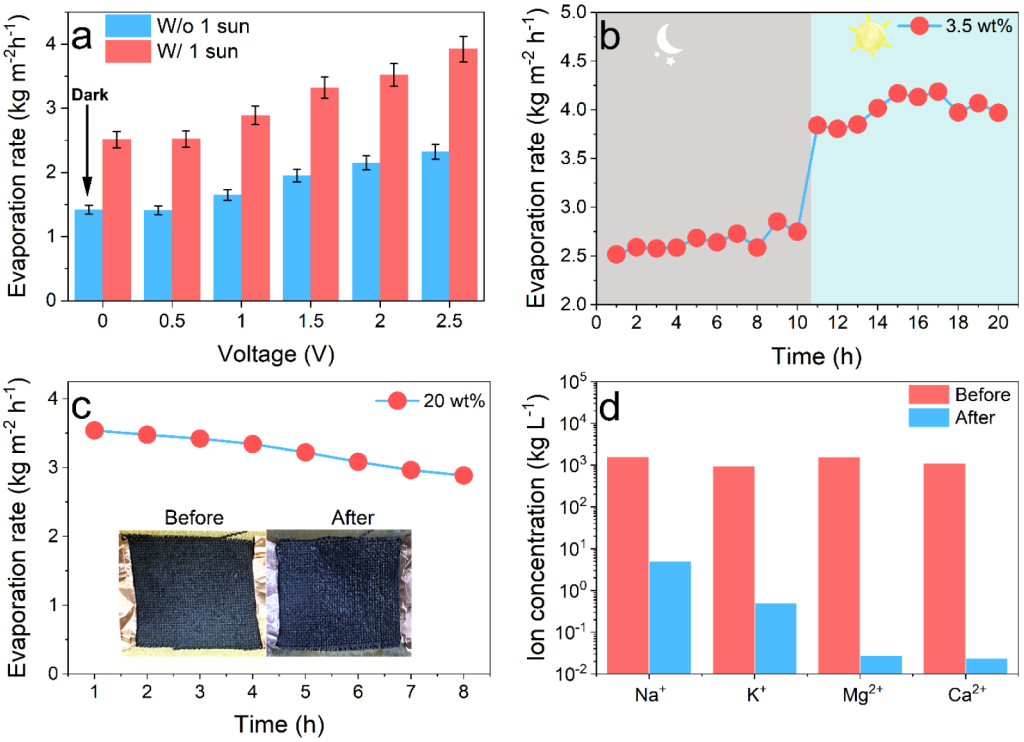

Figure 4. (a) Comparison of evaporation performance of SRGO−CF-5 for 3.5 wt % salt water. (b) Long-term evaporation performance of SRGO−CF-5 under conditions of 2.5 V (nighttime) and 1 sun and 2.5 V (daytime). (c) Evaporation rates under conditions of SRGO−CF-5 for 20 wt % hypersaline waters. Inset shows the images of SRGO−CF before and after evaporation. (d) Concentrations of 4 major ions of 3.5 wt % before and after desalination.

of SRGO−CF, which leads to the increase in radiative heating. According to the Stefan−Boltzmann law, the radiative heat transfer rate is proportional to the fourth power of the surface temperature ($P\alpha T^4$). This implies that even a small temperature increase causes a significant increase in radiative heating. Therefore, the supply of higher voltage can promote stronger thermal radiative heating, making it a promising approach for enhancing the evaporation performance in contactless evaporators. The present results demonstrate an excellent synergetic effect of photothermal heating and Joule heating-induced electrothermal heating in the SRGO−CF-5 evaporator. The combined effect of the increased surface temperature and enhanced radiative heating significantly boosts the overall evaporation performance. This synergy, further amplified by a higher input voltage, leads to stronger thermal radiative heating, making the SRGO−CF-5 evaporator highly effective for advanced heat-associated thermal applications.

The effect of standalone Joule heating in the SRGO−CF-5 evaporator was also evaluated under similar conditions, with varying input voltages from 0.5 to 2.5 V. As expected, the evaporation rates increase with voltage, achieving 2.77 kg m^{-2} h^{-1} at 2.5 V. IR thermal images (Figure S7) illustrate this evaporation performance, showing that the outer walls of the SRGO−CF reached a temperature of ∼39 °C after 30 min of continuous supply of 2.5 V DC power. Temperature gradients are formed along the walls, with cooler surface temperatures at higher elevations, compared to the surrounding environment. This indicates that a large portion of the walls gain heat from the surroundings, while a small section near the absorber experiences inevitable heat loss. The absorber itself reaches an average temperature of ∼42 °C within the same period, further demonstrating the impact of Joule heating on the evaporator's performance.

The results clearly demonstrate an increase in the surface temperature with the application of Joule heating voltages. Temporal variations of surface temperature in SRGO−CF, as shown in Figure 3d, reveal a rapid rise to 60 °C under 1 sun illumination within 2 min and stabilizing at 62 °C in 5 min. This localized heating is attributed to the excellent photothermal heat conversion efficiency of SRGO−CF and the low thermal conductivity of both SRGO−CF and the polyurethane sponge. A similar trend is observed with the addition of input voltages. The surface temperatures rapidly increased within 2 min, reaching 64.2 °C, 66.5 °C, 72.7 °C, 80.1 °C, and 86.9 °C at input voltages of 0.5 1, 1.5, 2, and 2.5 V, respectively. These elevated surface temperatures highlight the superior photothermal conversion and Joule heating-induced electrothermal heating of the SRGO−CF-5 device. As seen in the standalone Joule heating curve, the surface temperature at 2.5 V reaches nearly 60 °C, similar to the value achieved under 1 sun illumination. This implies that the supply of a 2.5 V input voltage can compensate for the reduced evaporation rates caused by low solar illumination, such as nighttime or cloudy conditions. Following the $I-V$ curve assessment of the proposed SRGO−CF evaporator, the enhancement of the evaporation performance driven by Joule heating was further evaluated. The $I-V$ curves, as shown in Figure S8, exhibit a linear relationship with increasing temperature, and the resistance of the SRGO−CF-5 evaporator was measured to be ∼4.6 Ω. This low resistance value is aligned with previous reports showcasing high steam generation performances.[19] For example, Wu et al. reported an MPC/cloth-F evaporator with a resistance of 7.96 Ω. They mentioned that the evaporator

https://doi.org/10.1021/acsami.4c17002
ACS Appl. Mater. Interfaces XXXX, XXX, XXX−XXX

needs to have a similar range of resistance to achieve high evaporation rates. The input power (P) is defined as $P = V^2/R$, where V represents the input voltage in volts and R denotes the resistance in ohms. Consequently, the input power is exponentially increased with input voltage, and the joule heating is subsequently increased according to Joule's Heating formula of $H = (P \times t)$, where H is the amount of heat generated in Joules and t is the elapsed time the input voltage is applied in seconds. The low resistance of the SRGO−CF-5 evaporator ensures efficient steam generation even at lower input voltages, as a higher input power leads to increased Joule heating. The joule heating mode of the SRGO−CF evaporator can compensate for reduced solar illumination, maintaining high evaporation rates even under unfavorable conditions, such as nighttime or cloudy environments. However, it is important to note that the efficiency of Joule heating is directly dependent on the applied voltage, and the overall evaporation performance of the evaporator is highly sensitive to its resistance values. Therefore, optimization of the resistance is crucial for maximizing heat generation and ensuring consistent evaporation in long-term operations. Table S2 shows the energy conversion efficiencies of the SRGO−CF-5 evaporator under different conditions. Under 1 sun solar illumination, the solar-to-vapor conversion efficiency is approximately 84%, which aligns well with the previously estimated overall heat loss of the evaporator. However, when the input voltage is applied, the evaporation rate increases while the efficiency decreases noticeably. This large drop in efficiency seems to be caused by unavoidable heat loss from the SRGO−CF evaporator to the copper wires connected to the DC power supply. However, this efficiency drop can be minimized through further optimization in the design of the SRGO−CF-5 evaporator to enhance its suitability for practical applications.

The impressive steam generation capacity of the SRGO−CF-5 device was tested for the desalination of seawater. By utilization of the low-voltage-assisted Joule heating method, the enhanced performance of salt-water evaporation and the all-day, all-weather capability of the evaporator were examined. Figure 4a showcases the evaporation performance of the fabricated SRGO−CF-5 evaporator for 3.5 wt % saltwater. To ensure consistent evaluation of evaporation performance at various power supplies, our desalination performance assessments were conducted using a standard laboratory power supply, as mentioned in the experimental section.

Since different power supplies have different power gradings, a comparison of the evaporation performance of Joule heating-induced evaporators would be difficult. Additionally, the aim of solar-based desalination is to minimize the impact of electrothermal heating and emphasize photothermal heating for sustainable solar-driven desalination. For 3.5 wt % saltwater, the SRGO−CF evaporator achieves an evaporation rate of 2.5 kg m^{-2} h^{-1} under 1 sun illumination. Similar to the water evaporation rates for pure water, the addition of input voltage increases the evaporation rates significantly. At 2.5 V and 1 sun illumination, the evaporation rate reaches as high as 3.52 kg m^{-2} h^{-1}. It should be noted that the evaporation rates are high, even at lower input voltages. To assess its suitability as an all-day, all-weather desalination device, we also examined the JHA electrothermal heating of SRGO−CF-5 was also examined. In the absence of photothermal heating, the SRGO−CF-5 can manage to evaporate saltwater up to a rate of 2.32 kg m^{-2} h^{-1} under 2.5 V input voltage. This implies that a solar still module employing the SRGO−CF-5 device can operate efficiently without excessive reliance on intense solar irradiation and weather conditions. These evaporation rates are consistent with those observed in previously reported contactless evaporators. (Table S3) To assess the all-day, all-weather capability of SRGO−CF-5, a long-term experiment was conducted under 2.5 V and 1 sun illumination, indicating daytime operation and 2.5 V as nighttime operation. As shown in Figure 4b, the evaporation performance remains constant throughout the experimentation period, confirming the practicability of the steam generator in all conditions. Furthermore, the evaporation performance was also evaluated for hypersaline brine with a concentration of >20 wt %, as shown in Figure 4c. High evaporation rates are obtained even for hypersaline brine with 20 wt % concentration. For all cases, the SRGO−CF evaporator is salt-free, demonstrating the antisalt fouling capability of the proposed SRGO−CF-5 evaporator (inset of Figure 4c).

The wall structure of SRGO−CF-5 can be utilized for zero liquid discharge (ZLD)-based salt collection. As saltwater ascends through the surrounding walls via evaporation-induced capillary action, salt can accumulate on the walls. Long-term operation demonstrates that salt accumulation does not hinder the evaporation performance at all. This is primarily due to the rapid water transport capability of the paper walls. In addition, the contactless design prevents salt fouling, which is a common issue in conventional ISSG evaporators. To further assess the antisalt fouling performance of SRGO−CF-5, a brine solution with a high concentration of ∼24 wt % was tested for 10 h under 1 sun illumination and 3 V input voltage. The SEM image presented in Figure S9 demonstrates the efficient salt collection capability of the proposed SRGO−CF-5 device, showcasing its potential for rapid ZLD-based salt harvesting. EDX analysis further confirmed the accumulation of salts, with an increasing concentration of Na^+ and Mg^{2+} ions deposited on the paper walls after the experiments, as shown in Figures S10 and S11. Furthermore, Figure 4d illustrates the ion concentrations of the four major ions before and after desalination. As expected, the freshwater samples exhibited ion concentrations at least three orders lower than those in seawater, confirming the desalination capability of the proposed SRGO−CF-5. The performance of SRGO−CF-5 was evaluated for practical applications, as shown in Figure S12. For comparison, a bare seawater system was also tested. The SRGO−CF-5 immediately showed fogging, indicating vapor collection on the surface, whereas the bare water system remained clear. With Joule heating, SRGO−CF-5 continued to generate steam at a steady rate of approximately 3 kg m^{-2} h^{-1}, even in foggy conditions, demonstrating its all-day, all-weather capability. Throughout the day-long test, the SRGO−CF-5 exhibited no salt fouling and produced significantly more condensed water than the bare water system.

The SRGO−CF-5 evaporator demonstrated several advantages over traditional solar-driven desalination systems. Its completely contactless design effectively prevents salt fouling, even at high salt concentrations, maintaining a consistent evaporation performance over extended periods. This antisalt fouling capability is crucial for long-term desalination applications, where salt buildup typically hampers efficiency in conventional systems. Additionally, the unique wall structure of SRGO−CF-5 enables effective salt collection through evaporation-induced capillary action, making it a viable solution for zero liquid discharge (ZLD) applications. The

https://doi.org/10.1021/acsami.4c17002
ACS Appl. Mater. Interfaces XXXX, XXX, XXX−XXX

device's integration of synergetic Joule heating further enhances its all-day, all-weather operation, enabling reliable desalination even in low sunlight conditions. This dual functionality—not only achieving efficient desalination but also enabling ZLD-based salt harvesting—highlights the SRGO−CF-5's potential as a versatile and highly innovative desalination device suitable for a wide range of environmental conditions.

CONCLUSION

A novel 3D contactless evaporator utilizing solar-reduced graphene oxide (SRGO) coated on CF is proposed for antisalt fouling, all-day, all-weather seawater desalination. The SRGO−CF evaporator efficiently harnesses solar energy and radiates heat to the surrounding paper walls, inducing radiative heating-based evaporation. The increased energy gain of the tall 3D paper walls enables the SRGO−CF evaporator to exceed the theoretical evaporation limit under 1 sun illumination. The addition of a low input voltage (2.5 V) further enhances the evaporation rate, reaching 4.27 kg m^{-2} h^{-1}. This is attributed to the synergistic photothermal and electrothermal properties of the SRGO−CF-5. In seawater desalination, the SRGO−CF-5 achieves an evaporation rate of 3.52 kg m^{-2} h^{-1} while demonstrating no salt fouling, a significant improvement over conventional ISSG evaporator. The proposed SRGO−CF-5 evaporator shows strong potential for salt harvesting through zero liquid discharge. Additionally, the consistent evaporation of this contactless evaporator without solar illumination enables it to be a promising candidate for continuous, all-weather desalination of brine water. This novel design addresses key challenges of conventional ISSG devices, such as a poor evaporation rate, weather dependency, and salt fouling. Therefore, the proposed contactless evaporator will give rise to significant advancements in the sustainable desalination of seawater.

ASSOCIATED CONTENT

Supporting Information

The Supporting Information is available free of charge at https://pubs.acs.org/doi/10.1021/acsami.4c17002.

XPS analysis, digital photographs of evaporator, SEM images of filter paper, IR thermal images of evaporator under different conditions, thermal efficiency and heat exchange calculations, *I*−*V* curve, SEM and EDX images of walls before and after desalination, and outdoor experiments (PDF)

AUTHOR INFORMATION

Corresponding Author

Sang J. Lee − *Department of Mechanical Engineering, Pohang University of Science and Technology, Pohang, Gyeongbuk 37673, The Republic of Korea;* orcid.org/0000-0003-3286-5941; Email: sjlee@postech.ac.kr

Authors

Higgins M. Wilson − *Department of Mechanical Engineering, Pohang University of Science and Technology, Pohang, Gyeongbuk 37673, The Republic of Korea*

Tawseef A. Wani − *Department of Chemical Engineering, Pohang University of Science and Technology, Pohang, Gyeongbuk 37673, The Republic of Korea*

Complete contact information is available at: https://pubs.acs.org/10.1021/acsami.4c17002

Author Contributions

The manuscript was written through contributions of all authors. All authors have given approval to the final version of the manuscript

Notes

The authors declare no competing financial interest.

ACKNOWLEDGMENTS

The authors thank the Korea Government for the financial support through the National Research Foundation of Korea (NRF) grant (MIST) (RS-2024-00341278).

REFERENCES

(1) Lewis, N. S. Research Opportunities to Advance Solar Energy Utilization. *Science* **2016**, *351* (6271), aad1920.

(2) Xu, Y.; Hu, J.; Zhang, X.; Yuan, D.; Duan, G.; Li, Y. Robust and Multifunctional Natural Polyphenolic Composites for Water Remediation. *Mater. Horiz.* **2022**, *9* (10), 2496−2517.

(3) Selvam, A.; Jain, G.; Chaudhuri, R. G.; Mandal, M. K.; Chakrabarti, S. Avant-Garde Solar−Thermal Nanostructures: Nascent Strategy into Effective Photothermal Desalination. *Sol. RRL* **2022**, *6* (n/a), 2200321.

(4) Liu, H.; Liu, L.; Fan, Z.; Liu, J.; Wang, H.; Wen, X.; Hu, G.; Liu, K.; Niu, R.; Gong, J. Transforming Waste Polyester into Porous Carbon Polyhedron for Interfacial Solar Steam and Hydrovoltaic Electricity Co-Generation. *Chem. Eng. J.* **2024**, *485*, 149690.

(5) Wu, X.; Chen, G. Y.; Owens, G.; Chu, D.; Xu, H. Photothermal Materials: A Key Platform Enabling Highly Efficient Water Evaporation Driven by Solar Energy. *Mater. Today Energy* **2019**, *12*, 277−296.

(6) Thoai, D. N.; Hoai Ta, Q. T.; Truong, T. T.; Van Nam, H.; Van Vo, G. Review on the Recent Development and Applications of Three Dimensional (3D) Photothermal Materials for Solar Evaporators. *J. Cleaner Prod.* **2021**, *293*, 126122.

(7) Wang, H.; Wen, X.; Liu, K.; Liu, Q.; Hu, G.; Liu, H.; She, Y.; Niu, R.; Tang, T.; Gong, J.Interfacial Solar-Driven Steam and Electricity Co-Generation Using Hydrangea-like Graphene by Salt-Assisted Carbonization of Waste Polylactic Acid. *SusMat*, **2024**, n/a, e242, .

(8) Niu, R.; Ren, J.; Koh, J. J.; Chen, L.; Gong, J.; Qu, J.; Xu, X.; Azadmanjiri, J.; Min, J. Bio-Inspired Sandwich-Structured All-Day-Round Solar Evaporator for Synergistic Clean Water and Electricity Generation. *Adv. Energy Mater.* **2023**, *13* (45), 2302451.

(9) Li, H.-N.; Yang, H.-C.; Zhu, C.-Y.; Wu, J.; Greiner, A.; Xu, Z.-K. A Self-Descaling Janus Nanofibrous Evaporator Enabled by a "Moving Interface" for Durable Solar-Driven Desalination of Hypersaline Water. *J. Mater. Chem. A* **2022**, *10* (39), 20856−20865.

(10) Ge, Y.; Su, Z.; Wang, L.; Wang, C.; Cai, P.; Lin, S.; Liu, Y.; Xu, S.; Bai, G. Self-Rotating Spherical Evaporator Based on Hydrogel and Black Titanium Oxide for Continuous Desalination of Seawater. *ACS Mater. Lett.* **2023**, *5* (9), 2576−2583.

(11) Li, L.; He, N.; Jiang, B.; Yu, K.; Zhang, Q.; Zhang, H.; Tang, D.; Song, Y. Highly Salt-Resistant 3D Hydrogel Evaporator for Continuous Solar Desalination via Localized Crystallization. *Adv. Funct. Mater.* **2021**, *31* (43), 2104380.

(12) Menon, A. K.; Haechler, I.; Kaur, S.; Lubner, S.; Prasher, R. S. Enhanced Solar Evaporation Using a Photo-Thermal Umbrella for Wastewater Management. *Nat. Sustainability* **2020**, *3* (2), 144−151.

(13) Chen, K.; Li, L.; Zhang, J. Design of a Separated Solar Interfacial Evaporation System for Simultaneous Water and Salt Collection. *ACS Appl. Mater. Interfaces* **2021**, *13* (49), 59518−59526.

(14) Chen, K.; Li, L.; Zhang, J. Long-Term Efficient Interfacial Solar Desalination Enabled by a Biomimetic 2D Water-Transport Structure Based on Silicone Nanofilaments. *ACS Appl. Energy Mater.* **2022**, *5* (10), 13031−13041.

(15) Su, J.; Chang, Q.; Xue, C.; Yang, J.; Hu, S. Sponge-Supported Reduced Graphene Oxides Enable Synergetic Photothermal and Electrothermal Conversion for Water Purification Coupling Hydrogen Peroxide Production. *Sol. RRL* **2022**, *6* (11), 2200767.
(16) Wu, J.; Li, X.; Zhang, T.; Li, X.; Li, W.; Yu, Z.-Z. All-Weather-Available Electrothermal and Solar−Thermal Wood-Derived Porous Carbon-Based Steam Generators for Highly Efficient Water Purification. *Mater. Chem. Front.* **2022**, *6* (3), 306−315.
(17) Xue, C.; Xue, R.; Huang, R.; Fan, X.; Zhang, H.; Zheng, W.; Li, Y.; Li, N.; Chang, Q.; Hu, S. Enhanced Interfacial Solar Driven Water Evaporation Performance of Ti Mesh through Growing TiO2 Nanotube and Applying Voltage. *Sep. Purif. Technol.* **2023**, *314*, 123633.
(18) Li, L.; Zhang, J. Highly Salt-Resistant and All-Weather Solar-Driven Interfacial Evaporators with Photothermal and Electrothermal Effects Based on Janus Graphene@silicone Sponges. *Nano Energy* **2021**, *81*, 105682.
(19) Liu, F.; Pang, H.; Gu, Y.; Ning, Y.; Bradley, R.; Zhao, B.; Wu, W. Electrically Powered Artificial Black Body for Low-Voltage High-Speed Interfacial Evaporation. *J. Mater. Chem. A* **2022**, *10* (43), 22992−23000.
(20) Arunkumar, T.; Wilson, H. M.; Lee, S. J. Waste Are in the Limelight: Cost-Effective Waste Materials for Sustainable Solar Desalination. *Clean Technol. Environ. Policy* **2023**, *25* (9), 2805−2830.
(21) Jian, H.; Wang, Y.; Li, W.; Ma, Y.; Wang, W.; Yu, D. Reduced Graphene Oxide Aerogel with the Dual-Cross-Linked Framework for Efficient Solar Steam Evaporation. *Colloids Surf., A* **2021**, *629*, 127440.
(22) Suranshe, S. S.; Patil, A. Strategically Improving Electrical Conductivity of Reduced Graphene Oxide through a Series of Reduction Processes. *Mater. Lett.* **2023**, *333*, 133648.
(23) Yar, A.; Dennis, J. O.; Yasin, A.; Din, F. U.; Irfan, M.; Khan, M. S.; Yang, C.-C.; Jose, R. The Solar Reduction of Graphene Oxide on a Large Scale for High Density Electrochemical Energy Storage. *Sustain. Energy Fuels* **2021**, *5* (10), 2724−2733.
(24) Bian, Y.; Ye, Z.; Zhao, G.; Tang, K.; Teng, Y.; Chen, S.; Zhao, L.; Yuan, X.; Zhu, S.; Ye, J.; Lu, H.; Yang, Y.; Fu, L.; Gu, S. Enhanced Contactless Salt-Collecting Solar Desalination. *ACS Appl. Mater. Interfaces* **2022**, *14* (29), 34151−34158.
(25) Ginting, R. T.; Abdullah, H.; Barus, D. A.; Fauzia, V. Extremely High-Efficiency Solar Steam Generation, Robust and Scalable Photothermal Evaporator Based on ZIF-67@MXene/rGO Decorated Rock Wool. *J. Mater. Chem. A* **2023**, *11* (10), 5296−5308.
(26) Ma, D.; Li, X.; Guo, Y.; Zeng, Y. Study on IR Properties of Reduced Graphene Oxide. *IOP Conf. Ser. Earth Environ. Sci.* **2018**, *108* (2), 022019.
(27) Mohanapriya, K.; Ghosh, G.; Jha, N. Solar Light Reduced Graphene as High Energy Density Supercapacitor and Capacitive Deionization Electrode. *Electrochim. Acta* **2016**, *209*, 719−729.
(28) Stobinski, L.; Lesiak, B.; Malolepszy, A.; Mazurkiewicz, M.; Mierzwa, B.; Zemek, J.; Jiricek, P.; Bieloshapka, I. Graphene Oxide and Reduced Graphene Oxide Studied by the XRD, TEM and Electron Spectroscopy Methods. *J. Electron Spectrosc. Relat. Phenom.* **2014**, *195*, 145−154.
(29) Pandit, T. P.; Wilson, H. M.; Lee, S. J. Joule-Heating Assisted Heliotropic Solar Steam Generator for All-Day, All-Weather Solar Desalination. *Desalination* **2024**, *573*, 117185.

https://doi.org/10.1021/acsami.4c17002
ACS Appl. Mater. Interfaces XXXX, XXX, XXX−XXX